

Observational Determination of the Turbulent Ambipolar Diffusion Scale and Magnetic Field Strength in Molecular Clouds

Talayeh Hezareh¹,

thezareh@uwo.ca

Martin Houde¹, Carolyn M^cCoey^{1,2}, and Hua-bai Li³

Abstract

We study the correlation of the velocity dispersion of the coexisting molecules H¹³CN and H¹³CO⁺ and the turbulent energy dissipation scale in the DR21(OH) star-forming region. The down-shift of the H¹³CO⁺ spectrum relative to H¹³CN is consistent with the presence of ambipolar diffusion at dissipation length scales that helps the process of turbulent energy dissipation, but at a different cut-off for ions compared to the neutrals. We use our observational data to calculate a turbulent ambipolar diffusion length scale $L' \simeq 17$ mpc and a strength of $B_{\text{pos}} \simeq 1.7$ mG for the plane of the sky component of the magnetic field in DR21(OH).

Subject headings: ISM: Clouds—ISM: Magnetic Fields—ISM: individual (DR21(OH))—Submillimeter—Physical Data and Processes: turbulence

1. Introduction

Interstellar magnetic fields and turbulence have been the most debated mechanisms of support against gravitational collapse in molecular clouds. Recent studies have evolved towards acknowledging both mechanisms by studying turbulence in a magnetized gas (e.g., Shebalin et al. 1983; Goldreich & Sridhar 1995; Ostriker et al. 2001; Biskamp 2003; Basu et al. 2009; Falceta-Gonçalves et al. 2010). It is, however, a challenge to combine the existing models for turbulence with observational data for the measurement of the interstellar magnetic fields to fully understand the dynamics in molecular clouds. There is yet no closed theory for magnetized turbulence due to its complicated and intermittent nature. On the other hand, interstellar magnetic fields are weak (\sim few hundred μ G to a few mG) and difficult to measure with the very few observational techniques currently at hand

¹The Department of Physics and Astronomy, The University of Western Ontario, London, Ontario, Canada N6A 3K7

²Department of Physics and Astronomy, University of Waterloo, 200 University Avenue W., Ontario, Canada N2L 3G1

³Max-Planck-Institut für Astronomie, Königstuhl 17, D-69117 Heidelberg, Germany

(e.g., Crutcher et al. 1999; Houde 2004; Falgarone et al. 2008; Hildebrand et al. 2009; Houde et al. 2009). It is therefore essential to innovate with more observing techniques to provide reliable data and test existing models.

Turbulence is basically a dissipative process. In an incompressible turbulent fluid, energy is transferred from large eddies to smaller ones, until it is dissipated by viscosity at small enough scales (Kolmogorov 1941). The dissipation of turbulent energy has important effects on the ISM, such as initiating collapse in supercritical cores (Basu et al. 2009), modifying the chemical evolution of the gas molecules (Xie et al. 1995), and causing the decoupling of gas and grains in a cloud (Falgarone & Puget 1995).

Li & Houde (2008) established a new observational technique, expanding on the original work of Houde et al. (2000a; 2000b) on the effect of magnetic fields on the spectral line widths of ion and neutral molecular species, to calculate the ambipolar diffusion length scale and the strength of the plane-of-the-sky component of the ambient magnetic field (B_{pos}) in molecular clouds. They studied the turbulent velocity dispersion spectra of a pair of coexistent ion and neutral molecular species (HCN and HCO^+) in M17, with the assumption that the turbulent energy dissipation process is associated with ambipolar diffusion.

In this paper, we explain the method of Li & Houde (2008) and our purpose to test their turbulent energy dissipation model using optically thin coexistent ion and neutral molecular species in §2, and present our observations in §3. The data analysis is explained in §4 and we end with a summary in §5.

2. The Method of Li & Houde (2008)

Ostriker et al. (2001) introduced a numerical method to study the kinetic structure in a single-fluid turbulent cloud by measuring the distribution of the velocity dispersion against the size and mass of the simulated regions over which it was averaged. They showed how the lower envelope of the calculated velocity dispersions depicts the actual turbulent velocity spectrum of the gas in their simulations. Li & Houde (2008) used this technique to study the velocity dispersions of HCN ($J = 4 \rightarrow 3$) and HCO^+ ($J = 4 \rightarrow 3$) spectral line profiles in M17 as a function of length scale. They noticed that the lower envelope of the HCO^+ data was consistently down-shifted from that of HCN by a constant amount, independent of scale, and interpreted this result as the signature of turbulent ambipolar diffusion acting at smaller spatial scales than probed by their observations. Based on these results Li & Houde (2008) suggested a scenario where ambipolar diffusion sets in at small enough length scales where neutrals decouple from the flux-frozen ions and the magnetic field, and the friction between the ions and the drifting neutrals causes the dissipation of turbulent energy. Tilley & Balsara (2010) tested this model by simulating a two-fluid (ion and neutral) turbulence with a range of different ionization fractions. Their results showed that at length scales comparable to the ambipolar diffusion scale certain MHD waves, including Alfvén waves, are strongly damped, and this

damping causes the velocity spectrum of ions to drop below that of the neutrals. They simulated ion and neutral spectral line profiles for ionization fractions ranging from 10^{-2} to 10^{-6} and plotted their corresponding velocity dispersions against different beam sizes, producing a result very similar to Li & Houde (2008). Thus they were successful in numerically duplicating the observational results of Li & Houde (2008), including their determination of the turbulent ambipolar diffusion scale.

Assuming the gas to be well coupled to the field lines at large scales and that ion-neutral decoupling occurs at dissipation length scales, Li & Houde (2008) obtained an expression for B_{pos} by setting the effective magnetic Reynolds number $R_m \sim V_n L / \beta$ to 1 at the decoupling length scale. Here $\beta = B^2 / 4\pi n_i \mu \nu_i$ is the effective magnetic diffusivity with n_i the ion density, ν_i the collision rate of an ion with the neutrals and μ the mean reduced mass characterizing such collisions. The aforementioned expression for B_{pos} is

$$B_{\text{pos}} = \left(\frac{L'}{0.5 \text{ mpc}} \right)^{1/2} \left(\frac{V'_n}{1 \text{ km s}^{-1}} \right)^{1/2} \left(\frac{n_n}{10^6 \text{ cm}^{-3}} \right) \left(\frac{\chi_e}{10^{-7}} \right)^{1/2} \text{ mG}, \quad (1)$$

where L' is the ion-neutral ambipolar diffusion decoupling length scale, V'_n the neutral velocity dispersion at L' , n_n the neutral volume density, and χ_e is the fractional ionization. It should be noted that Equation (1) provides only an approximate value for B_{pos} as it assumes that ambipolar diffusion sets in exactly when $R_m = 1$, which is most likely too simple an approximation. The decoupling scale and the velocity dispersion V'_n are determined by fitting the lower envelopes of the square of the ion and neutral velocity dispersion data (σ_i^2 and σ_n^2 , respectively) to Kolmogorov-type power laws. If the coexisting ions and neutral species are well coupled at large scales, their turbulent power spectra will have the same spectral index over the inertial range (i.e., at scales larger than the dissipation scale and smaller than the injection scale). Moreover, the cut-off range for the ion and neutral energy dissipation do not coincide, and assuming the ion energy spectrum to drop significantly at the ambipolar diffusion scale, the difference between σ_i^2 and σ_n^2 is the difference of the integral of the ion and neutral energy spectra between the ambipolar diffusion scale and neutral viscosity dissipation scale (this difference, a (see Equation 2 below), is the shaded area in Figure 3 of Li & Houde 2008). With all the above assumptions, the σ_i^2 and σ_n^2 data are thus fitted to the following expressions

$$\begin{aligned} \sigma_i^2(L) &= bL^n + a \\ \sigma_n^2(L) &= bL^n. \end{aligned} \quad (2)$$

The observational determination of velocity dispersions from spectral line profiles is a measurement of a velocity field that is integrated along the line of sight within a column of gas of volume $l^2 \times L$, where l is the beam size and L is the depth through the cloud. However, a given velocity field is associated with turbulent substructures that span volumes different than $l^2 \times L$. It should therefore be examined whether the observational value of σ^2 at a given beam size l truly represents the

actual velocity dispersion at that length scale. Falceta-Gonçalves et al. (2010) investigated this issue with spectral line profile synthesis and three-dimensional MHD numerical simulations. They showed that although the minimum observed velocity dispersions scale as the actual σ^2 , the coincidence of individual values at a given scale depends on l and the sonic Mach number of the system. The observed dispersion is generally a good approximation of the actual dispersion, although the latter is slightly underestimated for supersonic turbulence and overestimated for a subsonic regime. They also showed that the power law functions fitted to the lower envelopes and actual three-dimensional velocity dispersions from the simulations correspond well. The dispersions obtained using the lower envelope therefore appear to be reliable estimates for the actual velocity dispersions, as long as a large enough number of lines of sight are considered.

Li et al. (2010) studied the differences in the velocity dispersion for the spectral lines of H^{13}CN ($J = 1 \rightarrow 0$) and H^{13}CO^+ ($J = 1 \rightarrow 0$) in DR21(OH) using the data of Lai et al. (2003a). They performed a similar analysis for HCN ($J = 3 \rightarrow 2$) and HCO^+ ($J = 3 \rightarrow 2$) data they obtained with the Submillimeter Array in NGC 2024, and also HCN ($J = 4 \rightarrow 3$) and HCO^+ ($J = 4 \rightarrow 3$) lines previously observed by Houde et al. (2002) in M17 and used in Li & Houde (2008). In each source, the velocity dispersion comparisons were performed for two locations with measured B_{pos} line densities. They found that the ion-neutral velocity difference is almost constant in M17, which has a uniform density of magnetic field lines, while in NGC 2024 and DR21(OH) the ion-neutral velocity dispersion difference correlate well with the magnetic field line density. This behavior is predicted and consistent with the model of Li & Houde (2008). They also considered other possible parameters that could cause differences between the velocity dispersion of the two tracers, including optical depth, outflow enhancement, and presence of hyperfine structures in the spectral lines, but only turbulent ambipolar diffusion could consistently explain their observations.

The spectra of an HCN and HCO^+ pair, however, usually appear to be optically thick and are subject to saturation. The aim of this work is to test the turbulent energy dissipation model of Li & Houde (2008) with optically thin isotopologues i.e., H^{13}CN and H^{13}CO^+ , to investigate whether the constant down shift of the velocity dispersion spectrum of the ion from that of the neutral is consistently reproducible with different species. Accordingly, the lower optical depths of the aforementioned molecules will allow us to potentially probe magnetic fields at greater depths in star-forming regions, where they may be stronger (Li & Houde 2008; Basu 2000; Crutcher 1999). Also, just like their main isotopologues they have very similar molecular masses and the critical densities associated with their $J = 4 \rightarrow 3$ transition are approximately 10^7 cm^{-3} and 10^6 cm^{-3} , respectively. In particular, their line profiles will not be saturated or self absorbed, which is likely to be the case with HCN and HCO^+ , and therefore the calculated line widths will be better representatives of the true velocity dispersions characterizing the medium under study.

3. Observations

We obtained position-switch grid maps of $\text{H}^{13}\text{CN}(J = 4 \rightarrow 3)$ at 345.336 GHz and $\text{H}^{13}\text{CO}^+(J = 4 \rightarrow 3)$ at 346.998 GHz in weather grade 3 ($0.08 < \tau_{225} < 0.12$) in DR21(OH) during the months of August to November 2008 at the James Clerk Maxwell Telescope (JCMT) on the summit of Mauna Kea, Hawaii. The observations were performed using the HARP-B (Buckle et al. 2007) single sideband receiver and the ACSIS correlator configured for a bandwidth of 500 MHz and channel resolution of 61 kHz. HARP-B is a 4×4 element heterodyne focal plane array that uses SIS detectors. The 16 detectors have receiver temperatures of 94 – 165 K and are separated by $30''$ with a foot print of $2'$. To fully sample the $15''$ JCMT beam, we mapped with sample offsets of $15''$ around the reference position ($\alpha = 20^{\text{h}}39^{\text{m}}01^{\text{s}}$ and $\delta = 42^{\circ}22'37.7''$, J2000) of the source. Since the difference between the frequencies of $\text{H}^{13}\text{CN}(J = 4 \rightarrow 3)$ and $\text{H}^{13}\text{CO}^+(J = 4 \rightarrow 3)$ is 1.66 GHz, we made use of the special configuration capability of ACSIS to observe the two spectra simultaneously within the 1.8 GHz passband of the receiver. We used the previously published main beam efficiency of $\simeq 62\%$ determined with observations of Saturn at 345 GHz by Buckle et al. (2007).

4. Results

Figure 1 shows the intensity maps of $\text{H}^{13}\text{CN}(J = 4 \rightarrow 3)$ and $\text{H}^{13}\text{CO}^+(J = 4 \rightarrow 3)$, integrated over a velocity range of -20 km s^{-1} to 20 km s^{-1} in DR21(OH). The high critical density of the $J = 4 \rightarrow 3$ transition results in detection of radiation from high density regions only, as can be seen from the intensity contours congregating in an area of $\approx 40'' \times 40''$ around the reference position of the source. We performed the spectral line analysis with the Starlink¹ and Gildas² software packages. The spectra of neighboring regions were averaged across the maps to simulate beam sizes $15''$, $30''$, $45''$ and $60''$ at different lines of sight in the observed region. We then fitted multi-Gaussian profiles to each spectrum and the corresponding velocity dispersion σ was then calculated using these fits. The plot of the square of the velocity dispersions for which the dispersion is at least three times larger than its corresponding uncertainty is shown in the top panel of Figure 2 as a function of length scale, with the H^{13}CN data plotted in black and H^{13}CO^+ in red. We did not include the error bars in this plot for a clearer representation of the data points. The H^{13}CN data corresponding to the largest beam size are not shown, as they do not fit in the limits of the plot; we had low statistics at the $60''$ scale and therefore were not able to produce quantitative data points for either of the species at this scale. The presence of data points at each length scale above the lower envelopes can be associated with the interception of the corresponding line of sight with several turbulent substructures of different velocities that brings an increase in the observed velocity dispersions. Therefore, the minimum values for σ^2 may be attributed to the line of sight that

¹<http://starlink.jach.hawaii.edu>

²<http://iram.fr/IRAMFR/GILDAS/>

intercepts the fewest number of such turbulent sub-structures (Falceta-Gonçalves et al. 2010). All the minimum σ^2 values we obtained for both species arise from one location in DR21(OH), circled in red in Figure 1, thus further confirming the coexistence of H^{13}CN and H^{13}CO^+ and showing the specific region along the line of sight that contains the least number of turbulent substructures. The spectra for the different beam sizes at this location are displayed in Figure 3, with the H^{13}CO^+ profiles plotted in red and H^{13}CN in black and scaled to the temperature of H^{13}CO^+ for a clearer comparison of their line widths.

The lower envelopes of σ^2 for H^{13}CN and H^{13}CO^+ are plotted with their corresponding uncertainties in the bottom panel of Figure 2, with Kolmogorov-type power law fits given by Equation (2). As mentioned above, we did not have sufficient statistics to find the true lower envelope at the largest scale (i.e., $60''$) for both spectra and thus used the σ^2 data at the three smallest beam sizes for the power law fits. To enforce the same power law fit for both species, we first fitted the difference between the square of the velocity dispersion data of H^{13}CN and H^{13}CO^+ to a constant function to obtain a , and then fitted the sum of the two data sets to a power law of the form $2bL^n + a$ to obtain b and n . The fit results provide $a = -0.45 \pm 0.01 \text{ km}^2 \text{ s}^{-2}$, $b = 0.49 \pm 0.03 \text{ km}^2 \text{ s}^{-2} \text{ arcsecond}^{-n}$ and $n = 0.36 \pm 0.02$. Although our fit is not as equally good for the two species at all length scales as it was for Li & Houde (2008), it is still very satisfactory and perfectly adequate for our study. Assuming a significant drop in the ion velocity spectrum at the dissipation scale, the velocity dispersion of ions will be approximately equal to V'_n at L' i.e., $V'_n(L') \simeq \sigma_i^2(L')$. We can then write (Li & Houde 2008)

$$\begin{aligned} V_n'^2(L') &\simeq 0.37bnL'^n \\ &\simeq a + bL' \end{aligned} \tag{3}$$

and therefore

$$L'^n = -a/[b(1 - 0.37n)]. \tag{4}$$

Taking the distance from DR21(OH) to be 3 kpc (Genzel & Downes 1977), we obtain $L' \simeq 1.2''$ or $\simeq 17 \text{ mpc}$ and $V'_n \simeq 0.26 \text{ km s}^{-1}$.

We used the RADEX software package (Van der Tak et al. 2007) to calculate the gas volume density and optical depths associated with the $J = 4 \rightarrow 3$ transition of H^{13}CN and H^{13}CO^+ . Taking the values for the line widths and line temperatures of the spectral lines observed at the reference position of the source, and the column densities and excitation temperatures of the two species ($\simeq 10^{13} \text{ cm}^{-2}$ and $\simeq 13 \text{ K}$, respectively) from Hezareh et al. (2008), we get $n_n \simeq 10^6 \text{ cm}^{-3}$ and assuming the observed core to be as deep as it is wide, i.e., $40''$, we obtain $N(\text{H}_2) \simeq 2 \times 10^{24} \text{ cm}^{-3}$. Additionally, RADEX computes optical depths of 0.17 and 0.21 for H^{13}CN and H^{13}CO^+ lines, respectively. This optical depth comparison agrees with the discussion by Li et al. (2010) mentioned

earlier. We also use $\chi_e = 3.2 \times 10^{-8}$ for the ionization fraction as obtained by Hezareh et al. (2008) for DR21(OH). Applying the parameters above in Equation (1), we determine a value of $B_{\text{pos}} \simeq 1.7$ mG. This value can be inaccurate by a factor of a few due to the uncertainties in n_n and χ_e , and the fact that Equation (1) is derived with the aforementioned assumption of determining the turbulent ambipolar diffusion length scale by setting $R_m = 1$.

Our results are in general consistent with the calculations of Li & Houde (2008) although the measurements were done on different sources and with different pairs of molecular species. An exception is perhaps the measured turbulent ambipolar dissipation scale for M17 reported by Li & Houde (2008) was 1.8 mpc, almost an order of magnitude smaller than what we measure for DR21(OH). This, however, may simply be the result of a stronger magnetic field for our source. Indeed, using the same fractional ionization of 3.2×10^{-8} for M17 yields $B_{\text{pos}} \simeq 0.57$ mG for that source, approximately three times weaker than for DR21(OH). A relatively weaker field strength for M17 than for DR21(OH) is also corroborated with existing CN ($N = 1 \rightarrow 0$) Zeeman measurements (Crutcher et al. 1999; Falgarone et al. 2008). Furthermore, our result for B_{pos} is consistent with that of Lai et al. (2003b), who obtained a polarization map of dust emission in DR21(OH) and used the Chandrasekhar & Fermi (1953) method to calculate $B_{\text{pos}} \simeq 1$ mG.

We can now combine our value for B_{pos} with the Zeeman measurement of $B_{\text{los}} \simeq 0.4$ mG by Crutcher et al. (1999) in DR21(OH) and obtain a total strength of $B \simeq 1.8$ mG at a volume density $n(\text{H}_2) \simeq 10^6 \text{ cm}^{-3}$. We can also use this result to calculate a mass to flux ratio for the observed source. Taking $M/\Phi_B = 1.0 \times 10^{-20} N(\text{H}_2)/|B| \text{ cm}^2 \mu\text{G}$ (Mouschovias & Spitzer 1976) with $N(\text{H}_2) \simeq 2 \times 10^{24} \text{ cm}^{-2}$, we obtain $M/\Phi_B \simeq 10$, which implies that DR21(OH) exhibits a highly supercritical core. Although this number could be overestimated by the column density considering our assumption for the core geometry, it is consistent with the fact that DR21(OH) has indeed revealed signs of high-mass star formation. Detection of OH masers (Norris et al. 1982), H_2O masers (Genzel & Downes 1977), and high-velocity outflows from its two dense cores, MM1 and MM2 (Lai et al. 2003b), are indications of ongoing star formation in this source.

5. Summary & Discussion

We simultaneously observed and mapped H^{13}CN ($J = 4 \rightarrow 3$) and H^{13}CO^+ ($J = 4 \rightarrow 3$) in DR21(OH) to test the turbulent energy dissipation model of Li & Houde (2008). The down shift of the ion velocity dispersion spectrum from that of the neutral is readily explained by the presence of ambipolar diffusion that causes a steeper turbulent power spectrum for the ions compared to that of the neutrals at dissipation length scales (Li & Houde 2008). We used our observational data to calculate a turbulent ambipolar diffusion scale of $L' \simeq 17$ mpc and a plane of the sky magnetic field strength of $B_{\text{pos}} \simeq 1.7$ mG for this source.

Our analysis shows that the difference between the velocity dispersion of the optically thin H^{13}CN and H^{13}CO^+ spectral lines at different length scales exhibits a trend similar to the results

originally obtained by Li & Houde (2008) with the optically thick main isotopologues. It therefore follows that the ion line narrowing effect first discussed by Houde et al. (2000a) and the ensuing conclusions of Li & Houde (2008) cannot be due to a relative optical depth effect between the ion and neutral species. This further corroborates prior results from Houde et al. (2000b), which first investigated this possibility, and more recently those of Li et al. (2010).

Although, as previously mentioned that optically thin spectral lines are preferable for this analysis, it should be noted that H^{13}CN and H^{13}CO^+ are less abundant than the main species and are more difficult to map. Indeed, we observed the aforementioned pair in three additional sources DR21(Main), NGC2264 and NGC2068 but DR21(OH) was the only source in which we obtained enough detections away from the core to perform our analysis. Moreover, observing HCN and HCO^+ in regions where they are optically thick in the line core should not be too detrimental to the line width calculations, as the wings of such spectral lines are still optically thin and suitable for this study. More precisely, since the wings are more heavily weighted in line width calculations, the (multi-) Gaussian profiles fitted to such sections, away from the line peaks can be used for obtaining the velocity dispersions in both species (Li et al. 2010).

Finally, this technique has the advantage that it is not restricted to nearby sources, since the data analysis mainly involves line width calculations and does not require a spatial resolution high enough to resolve the ambipolar diffusion scale.

The authors thank the referee for providing helpful comments, and also S. Basu and W.Dapp for thoughtful discussions. M. H.'s research is funded through the NSERC Discovery Grant, Canada Research Chair, Canada Foundation for Innovation, Ontario Innovation Trust, and Western's Academic Development Fund programs.

REFERENCES

- Basu, S., Ciolek, G., E., Dapp, W. B., and Wurster, J. 2009, *New Astronomy*, 14, 483
- Basu, S. 2000, *ApJ*, 540, L103
- Biskamp, D. 2003, *Magnetohydrodynamic Turbulence* (Cambridge: Cambridge. Press)
- Buckle, J. V. et al. 2007, *MNRAS*, 399, 2, 1026
- Chandrasekhar, S., and Fermi, E. 1953, *ApJ*, 118, 113
- Crutcher, R. M. 1999, *ApJ*, 520, 706
- Crutcher, R. M., Troland, T. H., Lazareff, B., Paubert, G., and Kazès, I. 1999, *ApJ*, 514, 2, L121
- Falceta-Gonçalves, D., Lazarian, A., and Houde, M. 2010, *ApJ*, 713, 1376

- Falgarone, E., Troland, T. H., Crutcher, R. M., and Paubert, G. 2008, *A&A*, 487, 1, 247
- Falgarone E., and Puget J.-L. 1995, *A&A* 293 840
- Goldreich, P., and Sridhar, S. 1995, *ApJ*, 438, 763
- Genzel, R., and Downes, D. 1977, *A&AS*, 30, 145
- Hezareh, T., Houde, M., McCoey, C., Vastel, C., and Peng, R. 2008, *ApJ*, 684, 1221
- Hildebrand, R. H., Kirby, L., Dotson, J. L., Houde, M., and Vaillancourt, J. E. 2009, *ApJ*, 696, 567
- Houde, M., Bastien, P., Peng, R., Phillips, T. G., and Yoshida, H. 2000a, *ApJ*, 536, 857
- Houde, M., Peng, R., Phillips, T. G., Bastien, P., and Yoshida, H. 2000b, *ApJ*, 537, 245
- Houde, M., Bastien, P., Dotson, J. L., Dowell, C. D., Hildebrand, R. H., Peng, R., Phillips, T. G., Vaillancourt, J. E., and Yoshida, H. 2002, *ApJ*, 569, 803
- Houde, M. 2004, *ApJ*, 616L, 111
- Houde, M., Vaillancourt, J. E., Hildebrand, R. H., Chitsazzadeh, S., and Kirby, L. 2009, *ApJ*, 706, 1504
- Kolmogorov, A. N. 1941, *C.R. Acad. Sci. USSR.*, 30, 301
- Lai, S. P., Velusamy, T., and Langer, W. D. 2003a, *ApJ*, 596, 239
- Lai, S. P., Girart, J. M., and Crutcher, R. M. 2003b, *ApJ*, 598, 392
- Li, H., and Houde, M. 2008, *ApJ*, 677, 1151
- Li, H., Houde, M., Lai S. P., and Tirupati, T. K. 2010, *ApJ*, 718, 905
- Mouschovias, T. Ch., and Spitzer, L., Jr. 1976, *ApJ*, 210, 326
- Norris, R. P., Booth, R. S., Diamond, P. J., and Porter, N. D. 1982, *MNRAS* 201, 191
- Ostriker, E. C., Stone, J. M., and Gammie, C. F. 2001, *ApJ*, 546, 980
- Shebalin, J. V., Matthaeus, W. H., and Montgomery, D. 1983, *J. Plasma Phys.*, 29, 525
- Tilley, D. A., and Balsara, D. S. 2010, *MNRAS*, 406, 1201
- Van der Tak, F.F.S., Black, J. H., Schöier, F.L., Jansen, D.J., and van Dishoeck, E.F. 2007, *A&A* 468, 627-635.
- Xie T., Allen M., and Langer, W. D. 1995, *ApJ* 440, 674

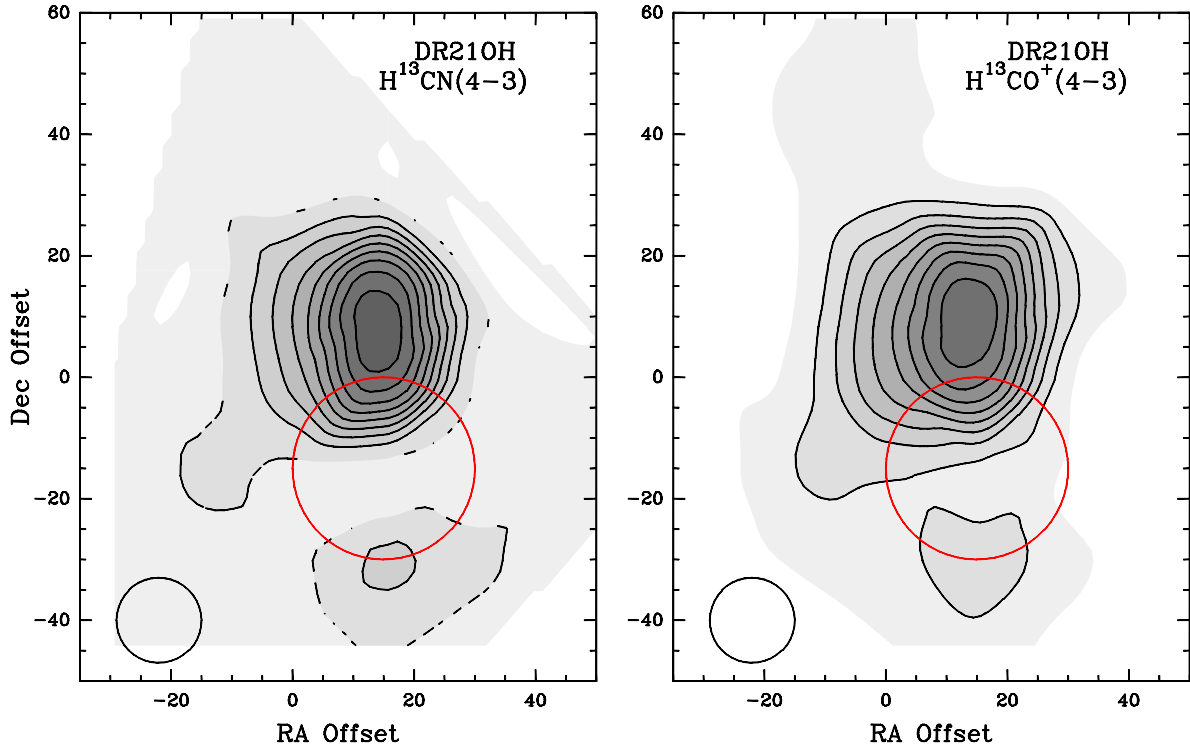


Fig. 1.— Comparison of the intensity maps of H^{13}CN and H^{13}CO^+ ($J = 4 \rightarrow 3$) integrated over a velocity range of -20 km s^{-1} to 20 km s^{-1} in DR21(OH). The contours span a range of 10% to 90% of the peak (9.03 K km s^{-1} for H^{13}CN and 8.23 K km s^{-1} for H^{13}CO^+) by increments of 10%. The red circles display the location along the line of sight where the minimum values of σ^2 are obtained observationally.

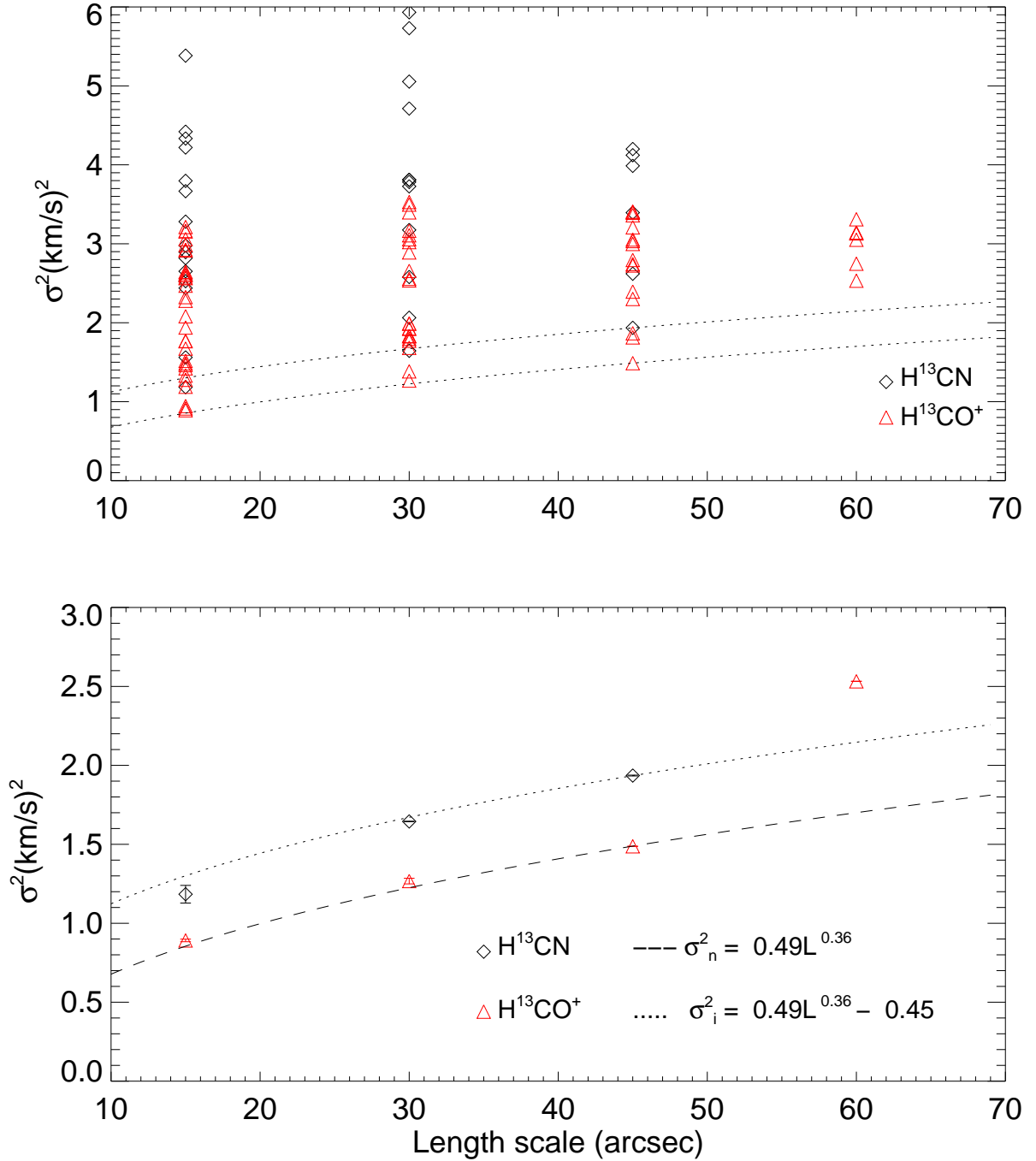


Fig. 2.— (*Top*) Plot of σ^2 as a function of length scale in DR21(OH). The error bars for the data points are not shown to avoid clutter in the graph. The values of σ^2 for H^{13}CN at $60''$ fall above the plot margin. (*Bottom*) The lower envelopes of the H^{13}CN and H^{13}CO^+ data fitted for Kolmogorov-type power laws.

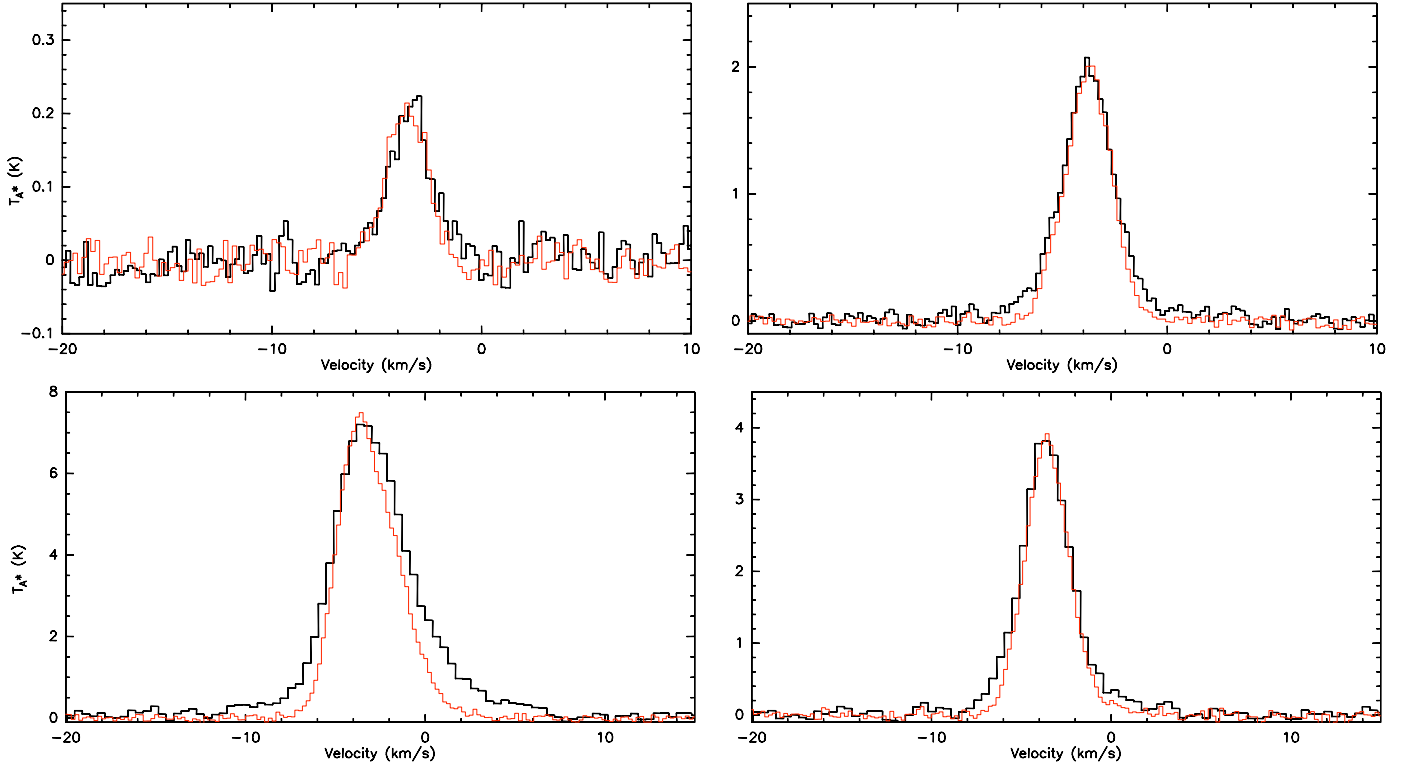


Fig. 3.— Comparison of the line widths of the $J = 4 \rightarrow 3$ transition of H^{13}CO^+ (red) and H^{13}CN (black) spectral lines corresponding to the minimum σ^2 values. Starting from top left, going clockwise are the spectra at beam sizes 15", 30", 45" and 60". In all the figures, the H^{13}CN lines are scaled to the H^{13}CO^+ line temperatures to provide a clearer comparison of the line widths.